PLEASE CITE THIS ARTICLE AS DOI: 10.1116/6.0002534

### Limiting Reagent Conditions to Control Inorganic Loading in $AlO_x$ – PET Hybrid Fabrics Created Through Vapor Phase Infiltration

Emily K. McGuinness\*+, Haley V. Manno\*+, Kira Pyronneau+, Benjamin C. Jean+, Nicole R. McClelland+, Mark D. Losego+#

\*School of Materials Science and Engineering, Georgia Institute of Technology, 771 Ferst Drive, Atlanta, GA 30332

\*These authors contributed equally to this work

#Corresponding Author: Mark D. Losego (<u>losego@gatech.edu</u>, 404-385-3630)

### **Abstract**

In this work, the vapor phase infiltration of polyethylene terephthalate (PET) fabrics with trimethylaluminum (TMA) and co-reaction with water vapor is explored as a function of limiting TMA conditions vs. excess TMA conditions at two infiltration temperatures. TMA is found to sorb rapidly into PET fibers, with a significant pressure drop occurring within seconds of TMA exposure. When large quantities of polymer are placed within the chamber, minimal residual precursor remains at the end of the pressure drop. This rapid and complete sorption facilitates the control of inorganic loading by purposely delivering a limited quantity of the TMA reagent. The inorganic loading for this system scales linearly with Precursor:C=O molar ratio up to 0.35 Precursor:C=O at 140 °C and 0.5 Precursor:C=O at 80 °C. After this point inorganic loading is constant irrespective of the amount of additional TMA reagent supplied. SEM analysis of pyrolyzed hybrids indicates this is likely due to the formation of an impermeable layer to

PLEASE CITE THIS ARTICLE AS DOI: 10.1116/6.0002534

subsequent infiltration as the core of the fibers remain uninfiltrated. The Precursor:C=O molar ratio in the sub-saturation regime is found to tune hybrid fabric morphology and material properties such as the optical properties of the fabric. Overall, this work demonstrates how a reagent-limited processing route can control the inorganic loading in VPI synthesized hybrid materials in a simpler manner than trying to control kinetics-driven methods.

**Keywords:** vapor phase infiltration, polyethylene terephthalate, limiting reagent, inorganic loading control, trimethylaluminum, organic-inorganic hybrid fabrics

### I. INTRODUCTION

Vapor phase infiltration (VPI) creates hybrid organic-inorganic materials from polymeric prefactors; modifying material properties while generally maintaining macroscale form. During VPI polymers are exposed to vapor-phase metalorganic or metal halide precursors that sorb within the polymer's subsurface and often are co-reacted with oxidants to create metal oxides. <sup>1-4</sup> Depending upon precursor chemistry, polymer chemistry, and VPI processing parameters, the physical and chemical structures of the hybrid material can be tuned. As a result, VPI has been studied for modifying a wide range of material properties including electrical conductivity, <sup>5-8</sup> mechanical strength, <sup>9-12</sup> degradation resistance (UV, <sup>13</sup> chemical, <sup>14, 15</sup> and thermal <sup>16</sup>), catalysis, <sup>17</sup> and photoluminescence. <sup>18-20</sup> Additionally, VPI has been employed as an inorganic templating <sup>21-27</sup> and phase contrast methodology. <sup>28-32</sup> Based upon these properties, VPI is of interest in a variety of industrial areas including solar cells, <sup>30, 33</sup> chemical separations, <sup>15, 34-38</sup> nanofabrication, <sup>21, 22, 39, 40</sup> and textile finishing. <sup>11, 13, 17, 41</sup>

PLEASE CITE THIS ARTICLE AS DOI: 10.1116/6.0002534

As many properties hinge upon the physical and chemical structure of the hybrid material, improved understanding of chemical reaction mechanisms, transport mechanisms, and thermodynamic driving forces in VPI as a function of precursor, polymer, and processing parameters is key. Progress in understanding chemical reaction mechanisms and their kinetics has been achieved using techniques such as *in situ* FTIR<sup>42-45</sup> and DFT computations<sup>45-48</sup> while transport and thermodynamic studies have leveraged *in situ* and *ex situ* spectroscopic ellipsometry, <sup>49-51</sup> *in situ* quartz crystal microbalance gravimetry, <sup>11, 44, 52, 53</sup> and *ex situ* inorganic loading, <sup>54</sup> yielding and applying several kinetically and thermodynamically informed models of the VPI process. <sup>48, 49, 55</sup> However, most of these works assume a sufficient quantity of precursor is supplied to fully saturate the polymer ("excess reagent") with few works featuring "limiting reagent" precursor conditions.

In this work, we explore how "limiting reagent" vs. "excess reagent" conditions influence the inorganic loading, physical structure, and optical properties of hybrid  $AlO_x$  / polyethylene terephthalate (PET) fabrics created through VPI with trimethylaluminum (TMA) and water vapor at two different infiltration temperatures. The TMA +  $H_2O$  VPI into PET system was chosen for this study due to its potential applications in the commodity textile dyeing and finishing industry as well as the wealth of prior knowledge regarding the transport, thermodynamics, and reaction mechanisms in this system. Previous work has also established that the stability to washing of the inorganic depends strongly on whether limiting precursor or excess precursor conditions are employed.<sup>41</sup>

PLEASE CITE THIS ARTICLE AS DOI: 10.1116/6.0002534

### II. EXPERIMENTAL

Creation of Hybrid AlOx - PET Fabrics through Vapor Phase Infiltration: Neat PET fabrics were obtained from TestFabrics (Spun Polyester Type 54, Disperse Dyeable) and were used as received. Infiltration of fabrics was performed in a custom-built box reactor using trimethylaluminum (TMA, bottle at room temperature, Strem Chemicals, 98%, DANGER: pyrophoric) and deionized water vapor dosed from a container at room temperature. The reactor design was described previously. 14, 15, 41 Fabrics were infiltrated with varying ratios of moles of TMA to moles of carbonyl functional group of the polymer fabric. The moles of TMA were calculated from calibration experiments conducted in an empty, heated reactor chamber to measure dose pressures based on precursor valve open time ("dose time", Figure S1, see supplementary material at [URL will be inserted by AIP Publishing]). From these experiments, the ideal gas law was applied to find the approximate moles of TMA using the temperature of the reactor walls and approximate chamber volume (1.5 cubic feet). Moles of carbonyl functionality were estimated via the fabric mass and molecular weight of the repeat unit (192.2 g/mol). Both moles of precursor and moles of carbonyl groups were varied to probe a wide range of Precursor:C=O molar ratios (3:1 to 1:140). An example calculation is provided in Table S1. Note that we use the term "moles of precursor" because TMA is known to dimerize in the gas phase, and the estimate of precursor delivered is based upon the ideal gas law from the chamber's measured pressure, which gives the number of "gaseous species" irrespective of if they are monomers or dimers. This choice is made because practitioners will find it easiest to also calculate the moles of precursors directly from their measured chamber pressure without needing to further estimate which

PLEASE CITE THIS ARTICLE AS DOI: 10.1116/6.0002534

fraction are dimerized—which would need to be done if the molar quantity of TMA or Al was desired (see SI).

For VPI processing, fabrics of varying mass were placed within the heated reactor which was then pumped down to approximately 30 mTorr with a rotary vane vacuum pump. All pressures in this work are measured with a Baratron capacitance manometer. The reactor was then purged with nitrogen at ~1.5 Torr for two hours to remove any sorbed water from the fabrics. The chamber was pumped down again, isolated, and the TMA precursor valve was opened for variable dose times. Fabrics were then exposed to the static TMA atmosphere for two hours. The chamber was purged again with nitrogen for one hour to remove excess TMA from the chamber environment. Fabrics were then exposed to DI water vapor (~2 to 2.5 Torr depending on room temperature) to co-react with TMA and leave an air stable hybrid material. Note: when large quantities of precursor (especially pyrophoric precursor) are sorbed it is imperative to ensure the final material is stable and safe for removal. Close pressure monitoring and review prior to sample removal is highly recommended. The water vapor was held in the isolated chamber for 2 hours. Then the chamber was purged with nitrogen for 5 minutes to remove any byproducts prior to hybrid fabric removal. The infiltration sequence was controlled via a custom-built control software described previously.49

In this study, fabrics were infiltrated at 80 and 140 °C. For hybrid fabrics created at infiltration temperatures of 80°C, the entire chamber was set to this temperature. For hybrid fabrics created at 140 °C, the chamber walls were set to 110 °C and a small portion at the bottom of the chamber was set to the higher temperature. Fabrics were placed in this hotter region. Representative

PLEASE CITE THIS ARTICLE AS DOI: 10.1116/6.0002534

pressure profiles for these processes are provided in Figure S2 (see supplementary material at [URL will be inserted by AIP Publishing].

Thermogravimetric Analysis: Inorganic loading of the hybrid fabrics was evaluated using thermogravimetric analysis (TGA, PerkinElmer TGA 4000). During each TGA measurement, 8-12 mg of hybrid fabric was heated in ~20 mL / min of flowing air to 120 °C and held at this temperature for 50 minutes to remove water. The mass after 50 min at 120 °C was used as the dry mass of the fabric. The fabrics were then heated at 10 °C / min to 700 °C, significantly beyond the complete degradation of neat PET . The TGA was then cooled to 120 °C at 20 °C / min and held at this temperature for at least 15 minutes to determine the inorganic mass alone. Inorganic weight percent loading is then calculated as the mass during the final 120 °C hold step divided by the fabric mass at the end of the initial drying period. Using 120 °C for both measurements reduces the influence of changes in air buoyancy that could influence the masses.

**UV-Vis Spectroscopy:** UV-Vis spectra were collected using an Avantes Starline AvaSpec 2048 detector with an integrating sphere containing a built-in halogen light source. Measurements were taken with the fabric of interest placed on top of a white reference tile purchased from Avantes. Prior to measurement, a dark spectrum was taken with a neat PET fabric placed on the tile and the light source turned off to get an accurate measurement of stray light. The light source was then turned on and allowed to warm up for 15 minutes. A reference spectrum was then taken using the white tile alone. The integrating time was set to the darkest color fabric and then maintained for all other experiments.

PLEASE CITE THIS ARTICLE AS DOI: 10.1116/6.0002534

Scanning Electron Microscopy / Energy Dispersive X-ray Spectroscopy: Imaging and elemental analysis of fabric cross-sections as well as imaging of "burned out" fabrics were performed with a Phenom ProX benchtop scanning electron microscope (SEM). Cross sections of hybrid fabrics were prepared for analysis by cryo-cutting in liquid nitrogen to avoid deforming the fibers. Images were scanned at 15 keV in backscatter mode. Energy dispersive x-ray (EDX) spectroscopy profiles were created using the same instrument.

**Digital Photography:** Photographs were taken with a Canon EOS Rebel T5i digital camera with a EFS 18-35 mm lens and image stabilizer under ambient light and a UV Lamp using an F-stop value of 5.6 for both conditions, a shutter-speed of 1/40 for UV and 1/15 for ambient, an ISO of 400 for UV and 800 for ambient, and a white balance setting of "cloudy" for UV and "white fluorescent" for ambient.

**Fabric Burnout:** The organic portion of hybrid fibers was removed by combusting in a box furnace at 700 °C for at least one hour. Fabrics were placed in box furnace during the ramp up, held at 700 °C for 1 h and then removed once the furnace was allowed to convectively cool to at least 100 °C.

### III. RESULTS AND DISCUSSION

To explore the role of limiting precursor vs. excess precursor conditions, the ratio of approximate moles of TMA to approximate moles of carbonyl functionality (the functional group known to chemically interact with TMA in VPI of PET)<sup>17, 19</sup> was varied during infiltration of PET fabrics with TMA and water vapor. The approximate number of moles TMA used in an infiltration was calculated using the ideal gas law. TMA vapor in equilibrium with its liquid was dosed from the

### © (1)

### cubic feet in volume) and the pressure was recorded using a Baratron capacitance manometer (example pressure vs. dose time values reported in Figure S1, see supplementary material at [URL will be inserted by AIP Publishing]). The moles of precursor were then calculated from the ideal gas law. Note that for this case the moles of "precursor" are the moles of molecules in the gas phase, which will be a mix of TMA monomers and dimers, but mostly dimers at these temperatures. The approximate number of moles of carbonyl functional groups was determined from the mass of the fabric placed within the chamber and the molar mass of the PET repeat unit PLEASE CITE THIS ARTICLE AS DOI: 10.1116/6.0002534 (192.2 g/mol). The ratio of these two values was then controlled by varying both the dose pressure and the mass of fabric. An example of these calculations is provided in Table S1 (see supplementary material at [URL will be inserted by AIP Publishing]. TMA is known to follow a two-step reaction mechanism when interacting with carbonyl

headspace of room temperature cylinder into a heated, evacuated chamber (approximately 1.5

functionalities with a rapid initial association step and a slower covalent bond formation. 44, 45, 52 Above ~110 °C the covalent bond formation occurs faster and within experimentally relevant timeframes for this work. To explore the influence of this reaction mechanism in combination with limiting reagent conditions two different heating conditions were used. For low temperature infiltrations, the chamber walls and sample stage area were all heated to 80 °C. For higher temperature infiltrations, chamber walls were heated to 110 °C while the sample stage area was heated to 140 °C. The differential heating was due to temperature restrictions on the valves of the chamber. For convenience, these conditions are referred to as 80 and 140 °C throughout.

# This is the author's peer reviewed, accepted manuscript. However, the online version of record will be different from this version once it has been copyedited and typeset PLEASE CITE THIS ARTICLE AS DOI: 10.1116/6.0002534

Figure 1a presents representative *in situ* pressure profiles for the TMA exposure step of the infiltration process with approximately 3:1, 1:1, and 1:3 Precursor:C=O conditions at 80 °C. For this particular set of representative experiments, the TMA dose pressure was kept constant at ~0.8 Torr for all three runs, while the quantity of fabric included in the chamber was varied to achieve different Precursor:C=O ratios. In this case, fabric masses of 0.05, 0.14, 0.52 grams were used. All pressure profiles in Figure 1a show an immediate rise in chamber pressure (due to the TMA dose) followed by a rapid drop in pressure, indicative of rapid sorption of the TMA into the PET fabric. However, the extent of this rapid drop in TMA chamber pressure varies with the quantity of fabric in the chamber. The total drop in TMA pressure is most dramatic for the run using the largest piece of fabric, and thus the smallest Precursor:C=O molar ratio. For this particular case, the 1:3 :C=O condition, the chamber pressure drops to near the background level within the first 10 min of the process, suggesting that nearly all of the TMA in chamber has been sorbed into the fabric and that the extent of the process reaction is limited by the quantity of TMA that has been supplied (i.e., reagent-limited).

Following infiltration, the inorganic loading of the hybrid fabrics was characterized via *ex situ* thermogravimetric analysis in air. Figure 1b plots the inorganic loading (weight percent) as a function of Precursor:C=O dosing ratio for both infiltration temperatures, with lines drawn to guide the eye. Here, the experimental conditions have been expanded to include a variety of fabric sizes and chamber process pressures, but these conditions have all been reduced to the respective Precursor:C=O molar ratio. Immediately evident is that at low Precursor:C=O molar ratios, inorganic loading varies with Precursor:C=O molar ratio, indicative of reagent-limited conditions. For infiltration at 80 °C, inorganic loading in this reagent-limited regime varies linearly

PLEASE CITE THIS ARTICLE AS DOI: 10.1116/6.0002534

with Precursor:C=O molar ratio until about a Precursor:C=O molar ratio of 0.5. Above this 0.5 Precursor:C=O molar ratio, the inorganic loading reaches a constant value of about 23 wt%. Similar behavior is observed for VPI at 140 °C, except the linear dependency continues to a Precursor:C=O molar ratio of only 0.35 and the inorganic loading saturates at only 17 wt%. For comparison, if all carbonyl sites within the fabric were saturated with a single TMA monomer (assuming no dimer presence), which upon reaction with water vapor formed Al(OH)<sub>3</sub>, the anticipated loading would be 81.2 wt% Al(OH)<sub>3</sub>. Note that this assumes no changes to polymer structure that would result in the loss of byproducts and a simplistic inorganic structure.

While within the linear portion, both temperatures exhibit a similar trend with a slope of about 48 wt% inorganic per 1 Precursor:C=O molar ratio unit (R² of 0.995). Following the initial linear increase in inorganic loading, the inorganic loading becomes relatively constant with subsequent increases in TMA reagent, with slight variations attributed to TGA measurement error. Within this linear portion, an opportunity exists for direct control of inorganic loading through either the mass of polymer supplied or the moles of precursor provided.

PLEASE CITE THIS ARTICLE AS DOI: 10.1116/6.0002534

### a)1.0 TMA Exposure Step **Dressure (Torr)**0.8 0.0 0.4 0.2 80 °C 3:1 Precursor:C=C 1:1 Precursor:C=C VPI Chamber PET fabric 1:3 Precursor:C=C 0.0 3 2 Time (hrs) **b)**30 80 °C 25 Weight Percent (%) 140 °C 20 15 5 \*lines are drawn to guide the eye 0 0 1 2 3 Precursor:C=O

**Figure 1.** a) *In situ* chamber pressure measured during the TMA exposure step of the VPI process for TMA infiltration into PET fabrics at Precursor:C=O molar ratios of 3:1, 1:1, and 1:3 at 80 °C with accompanying schematics demonstrating how fabric mass was used to vary the Precursor:C=O molar ratio. b) Inorganic loading measured by TGA as a function of Precursor:C=O molar ratio for AlO<sub>x</sub> / PET fabrics infiltrated at 80 and 140 °C. Lines are drawn to guide the eye.

Since the experimentally observed saturation weight loading at and above the 1:1 Precursor:C=O molar ratio is significantly lower than expected from simple estimations, we conducted a simple investigation as to whether the process was being inhibited from fully loading the fabric fibers.

PLEASE CITE THIS ARTICLE AS DOI: 10.1116/6.0002534

Combustion of these fibers provides evidence for infiltration being limited to the exterior portions of the fibers, as the remaining inorganics have a hollow-fiber like shape (**Figure S4**, see supplementary material at [URL will be inserted by AIP Publishing]). These results show that the inorganic never fully reaches the interior of these fibers, suggesting that the initially hybridized outer layer impedes subsequent precursor diffusion.

We hypothesize the mechanism for this incomplete infiltration is the formation of a hybrid layer that significantly impedes subsequent precursor diffusion. Our recently proposed reaction-diffusion model for the VPI process posits that precursors experience non-Fickian diffusion within a polymer during VPI. In many VPI systems, reactions of the sorbed precursor with the polymer create a new hybrid material with a different, typically lower, diffusion coefficient. In the reaction-diffusion model, this non-Fickian behavior is captured by assuming that the diffusivity becomes a function of the concentration of reacted species through a hindering factor. In certain cases, if the reaction of the precursors with the polymer occurs faster than precursors can diffuse into the polymer and the hindering is sufficiently high, then the outer hybrid layer can become impermeable to subsequent precursors.<sup>55</sup> In fact, prior literature has reported similar formation of impermeable layers in VPI treated PET fibers.<sup>18</sup>

An additional reason for the significant difference in inorganic loading from anticipated results may be a potential underestimation of the accessible polymer functional groups (we assume that all carbonyl groups can be accessed by TMA; however, small molecule penetrants notoriously have difficulties entering the crystalline regions of semi-crystalline polymers and crystallinity of PET has been previously shown to impact TMA infiltration<sup>11</sup>). The PET fabrics used in this work had approximately 32% crystallinity as measured by DSC.

PLEASE CITE THIS ARTICLE AS DOI: 10.1116/6.0002534

## Further, TMA exists as a dimer to varying extents depending upon temperature. If instead of considering moles of precursor delivered, moles of aluminum delivered are approximated from estimated fractions of monomer and dimer at both temperatures (see **Table S1** for calculations) we find the actual inorganic loadings to be even further below estimated values. Interestingly, when considering the inorganic loadings as a function of a ratio of moles of aluminum to moles of carbonyl (**Figure S3**), we find the saturation cutoffs move closer to a ratio of 1:1. However, the lack of complete infiltration of the PET fibers makes a quantitative fundamental conclusion challenging.

Returning to the results of Figure 1b, the similarity in inorganic uptake as a function of Precursor:C=O molar ratio regardless of infiltration temperature within the initial linear uptake regime is a somewhat surprising result. At higher temperatures, initial diffusion kinetics are expected to be faster, but so too are reaction kinetics leading to more rapid hindering and slower diffusion. <sup>55</sup> Additional factors include that 80 °C is below the glass transition temperature for PET while 140 °C is significantly above T<sub>g</sub>. Also, the reaction mechanism between TMA and the carbonyl group is also known to proceed through a rapid initial association occurring at all temperatures that is kinetically limited in its conversion to a covalent bond until heating past approximately 110 °C (reversing upon co-reaction with water vapor and leaving an unbound inorganic at low temperatures). Despite these differences, the inorganic loading dependency on Precursor:C=O molar ratio within the linear regime is independent of VPI process temperature. The similarity of the behaviors is indicative of an "equilibrium" process rather than a kinetics-limited process. Here, we posit that the same loading is reached independent of VPI process temperature because the loading is dictated only by the limited reagent, TMA. Irrespective of

PLEASE CITE THIS ARTICLE AS DOI: 10.1116/6.0002534

temperature, the fabric sorbs all of the TMA available, leading to the same amount of inorganic loading when Precursor:C=O molar ratio is kept constant. This result is characteristic of a reagent-limited process and may provide a more straightforward route to controlling inorganic loading than purely kinetics-driven processes.

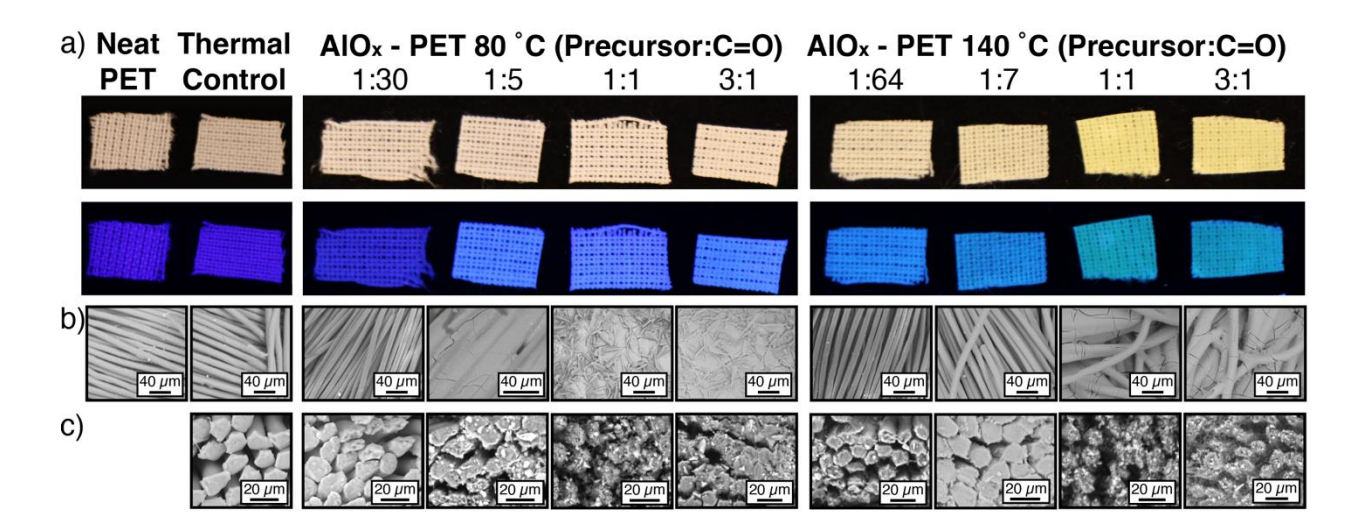


**Figure 2.** Neat PET, thermal control PET, and hybrid PET fabrics prepared at 80 and 140 °C with varying Precursor:C=O molar ratios as imaged by a) digital camera under ambient and UV lighting b) SEM in plan view and c) SEM of cryo-cut fabric cross sections.

To understand the role this difference in inorganic loading has on the physical structure and optical properties of hybrid  $AlO_x$  / PET fabrics, images were taken with SEM as well as a digital camera under both ambient and UV light sources (**Figure 2**). Consistent with prior literature reports, **Figure 2a** shows both the color and photoluminescence progression that occurs as both inorganic quantity and infiltration temperature increases. <sup>17, 19, 20, 41</sup> **Figure 2b** shows plan-view SEM images highlighting the morphological differences for neat PET, thermal control PET, and hybrid  $AlO_x$  / PET fabrics created with a range of Precursor:C=O molar ratios at 80 and 140 °C. Neat PET and thermal control fabrics appear identical. For both 80 and 140 °C, hybrid fabrics

PLEASE CITE THIS ARTICLE AS DOI: 10.1116/6.0002534

prepared within the linear regime of the Precursor:C=O molar versus inorganic loading curve largely maintain their original structure. As Precursor:C=O molar ratio increases, the fibers become more brittle (or ceramic-like) in appearance, as indicated by the formation of cracks on the fiber surfaces. Outside of the linear regime, fibers at both temperatures begin to sinter together with neighbors creating a monolithic yarn at 80 °C and a highly connected fibrous structure at 140 °C. However, in cross-section (**Figure 2c**) all hybrid fabrics retain some degree of their fibrous nature even within the highly connected structures.

The transition from fabric-like to highly connected as a function of Precursor:C=O and inorganic loading may be driven by a number of sources including melting due to the highly exothermic nature of the reactions taking place, the significant swelling of polymers that often occurs with VPI, or the desorption of water vapor forming a purely inorganic coating. However, this last mechanism is unlikely as EDX mapping reveals a significant quantity of carbon signal indicating even the ceramic-like monoliths maintain a hybrid structure rather than purely inorganic coatings, as shown in **Figure S5** (See supplementary material at [URL will be inserted by AIP Publishing]. Overall, the structural changes as a function of Precursor:C=O open an avenue for optimization between hybrid material property changes and maintenance of macroscale structure.

PLEASE CITE THIS ARTICLE AS DOI: 10.1116/6.0002534

### a) 3:1 1.2 2:1 1:103 1:137 **Absorbance** Neat PET 0.8 0.6 0.4 AIO<sub>x</sub> / PET 80 °C 0.2 450 500 550 400 600 Wavelength (nm) b) 2:1 1.2 1:1 1:64 1:113 Absorbance Neat PET 0.8 0.6 0.4 AIO, / PET 140°C 500 550 600 300 350 Wavelength (nm)

**Figure 3.** UV-vis spectra of hybrid AlOx / PET fabrics created at a) 80 °C and b) 140 °C with varying Precursor:C=O molar ratios.

One such tunable property shift that has been previously reported for hybrid  $AlO_x$  / PET fabrics is the photoluminescence and color of the hybrid material. Akyildiz *et al.* reported the ability to control the photoluminescence of hybrid  $AlO_x$  / PET fabrics via both temperature and sequential vapor infiltration (SVI) cycle number.<sup>17, 19, 20</sup> Similar to their findings, a shift in color and increase in photoluminescence is observed with inorganic loading (via limiting reagent) and temperature as shown in **Figure 3a**. This shift in optical properties is quantified via UV-Vis in **Figure 3**. Foremost, the observed difference in saturation and color is significantly driven by infiltration temperature. However, for both 80 and 140 °C, the shift in optical properties is tunable under limiting reagent stoichiometries, but reaches a steady state once inorganic loading is saturated.

PLEASE CITE THIS ARTICLE AS DOI: 10.1116/6.0002534

For comparable Precursor:C=O molar ratios, the absorption at 140 °C is stronger than at 80 °C likely highlighting a significant contribution of the covalently bound state to the optical properties of this system. Overall, the optical properties of this system demonstrate a tunability with Precursor:C=O molar ratio. This demonstration suggests that using the limited-reagent processing regime in VPI can be a route to control inorganic loading and engineer desired material properties in these hybrid materials.

### IV. SUMMARY AND CONCLUSIONS

Controlling inorganic loading in VPI is critical to designing the properties of the resultant hybrid materials. In this work, an additional mechanism for controlling inorganic loading is demonstrated: the use of limiting reagent conditions. By exploring the relative ratio of TMA to carbonyl functionality in the infiltration of PET fabrics at two temperatures, we demonstrate the ability to use a limiting reagent to control inorganic loading up to a critical concentration beyond which the system likely forms an impermeable barrier to subsequent precursor sorption. The loading of inorganic with limiting reagent conditions is independent of process temperature, but the saturation point does vary with process temperature. Hence, in the reagent limited regime, inorganic loading is largely independent of process conditions (e.g., process temperature), making it easier to achieve a specific inorganic loading fraction than trying to control a kineticsdriven process. Similar behavior is expected in other systems, although true solubility points may be reachable at saturation if an impermeable barrier does not form. In these cases, differences in the solubility limit with process temperature are also expected to alter the saturation values. We further demonstrate that the optical properties of these hybrid fabrics vary monotonically throughout the reagent limited process regime where inorganic loading varies, but these

PLEASE CITE THIS ARTICLE AS DOI: 10.1116/6.0002534

properties become constant when process conditions exceed the critical saturation concentration. These results provide an important new route to process control and structure design in VPI-synthesized hybrid materials.

### **Acknowledgements**

H.V.M, B.C.J., K.P., and N.R.M were supported in part by the Georgia Tech President's Undergraduate Research Award (PURA) and the Roxanne D. Westendorf Undergraduate Research Fund. B.C.J., E.K.M., and M.D.L. also received support from the National Science Foundation (DMREF-1921873). E.K.M. was also supported by the Department of Defense (DoD) through the National Defense Science & Engineering Graduate (NDSEG) Fellowship Program. Part of this research was conducted in Georgia Tech's Materials Innovation & Learning Laboratory (The MILL), an uncommon "make and measure" space committed to elevating undergraduate research in materials science.

### Data Availability:

Data is available upon request, please write the corresponding author.

### **Conflicts of Interest**

The authors have no conflicts to disclose.

This is the author's peer reviewed, accepted manuscript. However, the online version of record will be different from this version once it has been copyedited and typeset. PLEASE CITE THIS ARTICLE AS DOI: 10.1116/6.0002534

### **REFERENCES**

- 1. R. Z. Waldman, D. J. Mandia, A. Yanguas-Gil, A. B. F. Martinson, J. W. Elam and S. B. Darling, J. Chem. Phys. **151** (19), 190901 (2019).
- 2. C. Z. Leng and M. D. Losego, Mater. Horizons 4 (5), 747-771 (2017).
- 3. K. Ashurbekova, K. Ashurbekova, G. Botta, O. Yurkevich and M. Knez, Nanotechnology **31** (34), 342001 (2020).
- 4. I. Azpitarte and M. Knez, MRS Commun. 8 (3), 727-741 (2018).
- 5. S. A. Gregory, Y. Li, T. D. Monroe, J. Li, S. K. Yee and M. D. Losego, ACS Appl. Polym. Mater. **3** (2), 720-729 (2021).
- 6. W. Wang, C. Chen, C. Tollan, F. Yang, M. Beltran, Y. Qin and M. Knez, ACS Appl. Mater. Interfaces **9** (33), 27964-27971 (2017).
- 7. W. Wang, C. Chen, C. Tollan, F. Yang, Y. Qin and M. Knez, J. Mater. Chem. C **5** (10), 2686-2694 (2017).
- 8. W. K. Wang, F. Yang, C. Q. Chen, L. B. Zhang, Y. Qin and M. Knez, Adv. Mater. Interfaces **4** (4), 1600806-1600806 (2017).
- 9. S.-M. Lee, E. Pippel, O. Moutanabbir, I. Gunkel, T. Thurn-Albrecht and M. Knez, ACS Appl. Mater. Interfaces **2** (8), 2436-2441 (2010).
- 10. S. M. Lee, E. Pippel, U. Gosele, C. Dresbach, Y. Qin, C. V. Chandran, T. Brauniger, G. Hause and M. Knez, Science **324** (5926), 488-492 (2009).
- 11. R. P. Padbury and J. S. Jur, J Vac Sci Technol A **33** (1), 9 (2015).
- 12. Y. J. Sun, R. P. Padbury, H. I. Akyildiz, M. P. Goertz, J. A. Palmer and J. S. Jur, Chem. Vapor Depos. **19** (4-6), 134-141 (2013).
- 13. I. Azpitarte, A. Zuzuarregui, H. Ablat, L. Ruiz-Rubio, A. Lopez-Ortega, S. D. Elliott and M. Knez, Chem. Mat. **29** (23), 10068-10074 (2017).
- 14. E. K. McGuinness, C. Z. Leng and M. D. Losego, ACS Appl. Polym. Mater. 2 (3), 1335-1344 (2020).
- 15. E. K. McGuinness, F. Y. Zhang, Y. Ma, R. P. Lively and M. D. Losego, Chem. Mat. **31** (15), 5509-5518 (2019).
- 16. J. T. Bamford, R. A. Smith, C. Z. Leng, W. R. Gutekunst and M. D. Losego, Macromolecules **54** (14), 6790-6798 (2021).
- 17. H. I. Akyildiz, K. L. Stano, A. T. Roberts, H. O. Everitt and J. S. Jur, Langmuir **32** (17), 4289-4296 (2016).
- 18. H. I. Akyildiz and J. S. Jur, J. Vac. Sci. Technol. A **33** (2), 5 (2015).
- 19. H. I. Akyildiz, M. Lo, E. Dillon, A. T. Roberts, H. O. Everitt and J. S. Jur, J. Mater. Res. **29** (23), 2817-2826 (2014).
- 20. H. I. Akvildiz, M. B. M. Mousa and J. S. Jur, J. Appl. Phys. **117** (4), 7 (2015).
- 21. D. Berman and E. Shevchenko, J. Mater. Chem. C 8 (31), 10604-10627 (2020).
- 22. R. Azoulay, N. Shomrat, I. Weisbord, G. Atiya and T. Segal-Peretz, Small 15 (51), e1904657 (2019).
- 23. O. M. Ishchenko, S. Krishnamoorthy, N. Valle, J. Guillot, P. Turek, I. Fechete and D. Lenoble, J. Phys. Chem. C **120** (13), 7067-7076 (2016).
- 24. J. Kamcev, D. S. Germack, D. Nykypanchuk, R. B. Grubbs, C. Y. Nam and C. T. Black, ACS Nano **7** (1), 339-346 (2013).
- 25. Q. Peng, Y. C. Tseng, S. B. Darling and J. W. Elam, ACS Nano **5** (6), 4600-4606 (2011).
- 26. Y. C. Tseng, Q. Peng, L. E. Ocola, J. W. Elam and S. B. Darling, J. Phys. Chem. C **115** (36), 17725-17729 (2011).
- 27. D. H. Yi, C. Y. Nam, G. Doerk, C. T. Black and R. B. Grubbs, ACS Appl. Polym. Mater. **1** (4), 672-683 (2019).

the online version of record will be different from this version once it has been copyedited and typeset

This is the author's peer reviewed, accepted manuscript. However, the online version of record will be diff PLEASE CITE THIS ARTICLE AS DOI: 10.1116/6.0002534

- 28. T. Segal-Peretz, J. Winterstein, M. Doxastakis, A. Ramirez-Hernandez, M. Biswas, J. Ren, H. S. Suh, S. B. Darling, J. A. Liddle, J. W. Elam, J. J. de Pablo, N. J. Zaluzec and P. F. Nealey, ACS Nano **9** (5), 5333-5347 (2015).
- 29. T. Segal-Peretz, C. Zhou, J. X. Ren, T. Dazai, L. E. Ocola, R. N. S. Divan and P. F. Nealey, J. Photopolym. Sci. Tec. **29** (5), 653-657 (2016).
- 30. O. Nahor, T. Segal-Peretz, L. Neeman, D. Oron and G. L. Frey, J. Mater. Chem. C **2** (21), 4167-4176 (2014).
- 31. S. Obuchovsky, M. Levin, A. Levitsky and G. L. Frey, Org. Electron. 49, 234-241 (2017).
- 32. S. Obuchovsky, B. Shamieh, I. Deckman, G. Ankonina and G. L. Frey, Sol. Energy Mater. Sol. Cells **143**, 280-283 (2015).
- 33. S. Obuchovsky, I. Deckman, M. Moshonov, T. S. Peretz, G. Ankonina, T. J. Savenije and G. L. Frey, J. Mater. Chem. C **2** (42), 8903-8910 (2014).
- 34. D. S. Bergsman, B. A. Getachew, C. B. Cooper and J. C. Grossman, Nat. Commun **11** (1), 3636 (2020).
- 35. X. Chen, L. Wu, H. Yang, Y. Qin, X. Ma and N. Li, Angew. Chem. Int. Edit. **60** (33), 17875-17880 (2021).
- 36. W. Ogieglo, T. Puspasari, M. K. Hota, N. Wehbe, H. N. Alshareef and I. Pinnau, Mater. Today Nano **9**, 100065-100065 (2020).
- 37. R. Z. Waldman, D. Choudhury, D. J. Mandia, J. W. Elam, P. F. Nealey, A. B. F. Martinson and S. B. Darling, JOM **71** (1), 212-223 (2019).
- 38. C. Zhou, T. Segal-Peretz, M. E. Oruc, H. S. Suh, G. Wu and P. F. Nealey, Adv. Funct. Mater. **27** (34), 1701756 (2017).
- 39. J. W. Choi, Z. Li, C. T. Black, D. P. Sweat, X. Wang and P. Gopalan, Nanoscale **8** (22), 11595-11601 (2016).
- 40. N. Tiwale, A. Subramanian, K. Kisslinger, M. Lu, J. Y. Kim, A. Stein and C. Y. Nam, J. Mater. Chem. C **7** (29), 8803-8812 (2019).
- 41. K. Pyronneau, E. K. McGuinness, A. J. Gonzalez, B. C. Jean, H. V. Manno, N. R. McClelland and M. D. Losego, ACS Appl. Polym. Mater. (2022).
- 42. M. Biswas, J. A. Libera, S. B. Darling and J. W. Elam, J. Phys. Chem. C **119** (26), 14585-14592 (2015).
- 43. B. Gong and G. N. Parsons, J. Mater. Chem. **22** (31), 15672-15682 (2012).
- 44. E. C. Dandley, C. D. Needham, P. S. Williams, A. H. Brozena, C. J. Oldham and G. N. Parsons, J. Mater. Chem. C **2** (44), 9416-9424 (2014).
- 45. G. T. Hill, D. T. Lee, P. S. Williams, C. D. Needham, E. C. Dandley, C. J. Oldham and G. N. Parsons, J. Phys. Chem. C **123** (26), 16146-16152 (2019).
- 46. Y. Liu, E. K. McGuinness, B. C. Jean, Y. Li, Y. Ren, B. G. d. Rio, R. P. Lively, M. D. Losego and R. Ramprasad, J. Phys. Chem. B **126** (31), 5920-5930 (2022).
- 47. N. Sasao, S. Sugimura and K. Asakawa, JPN J. Appl. Phys. **59** (SI), SIICO2 (2020).
- 48. N. Sasao, S. Sugimura and K. Asakawa, JPN J. Appl. Phys. **60** (SC), SCCC04 (2021).
- 49. C. Z. Leng and M. D. Losego, Phys Chem Chem Phys **20** (33), 21506-21514 (2018).
- 50. F. E. Caligiore, D. Nazzari, E. Cianci, K. Sparnacci, M. Laus, M. Perego and G. Seguini, Adv. Mater. Interfaces 6 (12), 1900503-1900503 (2019).
- 51. E. Cianci, D. Nazzari, G. Seguini and M. Perego, Adv. Mater. Interfaces **5** (20), 1801016-1801016 (2018).
- 52. J. W. Elam, M. Biswas, S. Darling, A. Yanguas-Gil, J. D. Emery, A. B. F. Martinson, P. F. Nealey, T. Segal-Peretz, Q. Peng, J. Winterstein, J. A. Liddle and Y. C. Tseng, ECS Transactions **69** (7), 147-157 (2015).
- 53. R. P. Padbury and J. S. Jur, Langmuir **30** (30), 9228-9238 (2014).
- 54. B. C. Jean, Y. Ren, E. K. McGuinness, R. P. Lively and M. D. Losego, Mater. Chem. Phys. **290**, 126577 (2022).

## ACCEPTED MANUSCRIPT

### Journal of Vacuum Science & Technology A



This is the author's peer reviewed, accepted manuscript. However, the online version of record will be different from this version once it has been copyedited and typeset.

PLEASE CITE THIS ARTICLE AS DOI: 10.1116/6.0002534

55. Y. Ren, E. K. McGuinness, C. Huang, V. R. Joseph, R. P. Lively and M. D. Losego, Chem. Mat. **33** (13), 5210-5222 (2021).

# ACCEPTED MANUSCRIPT

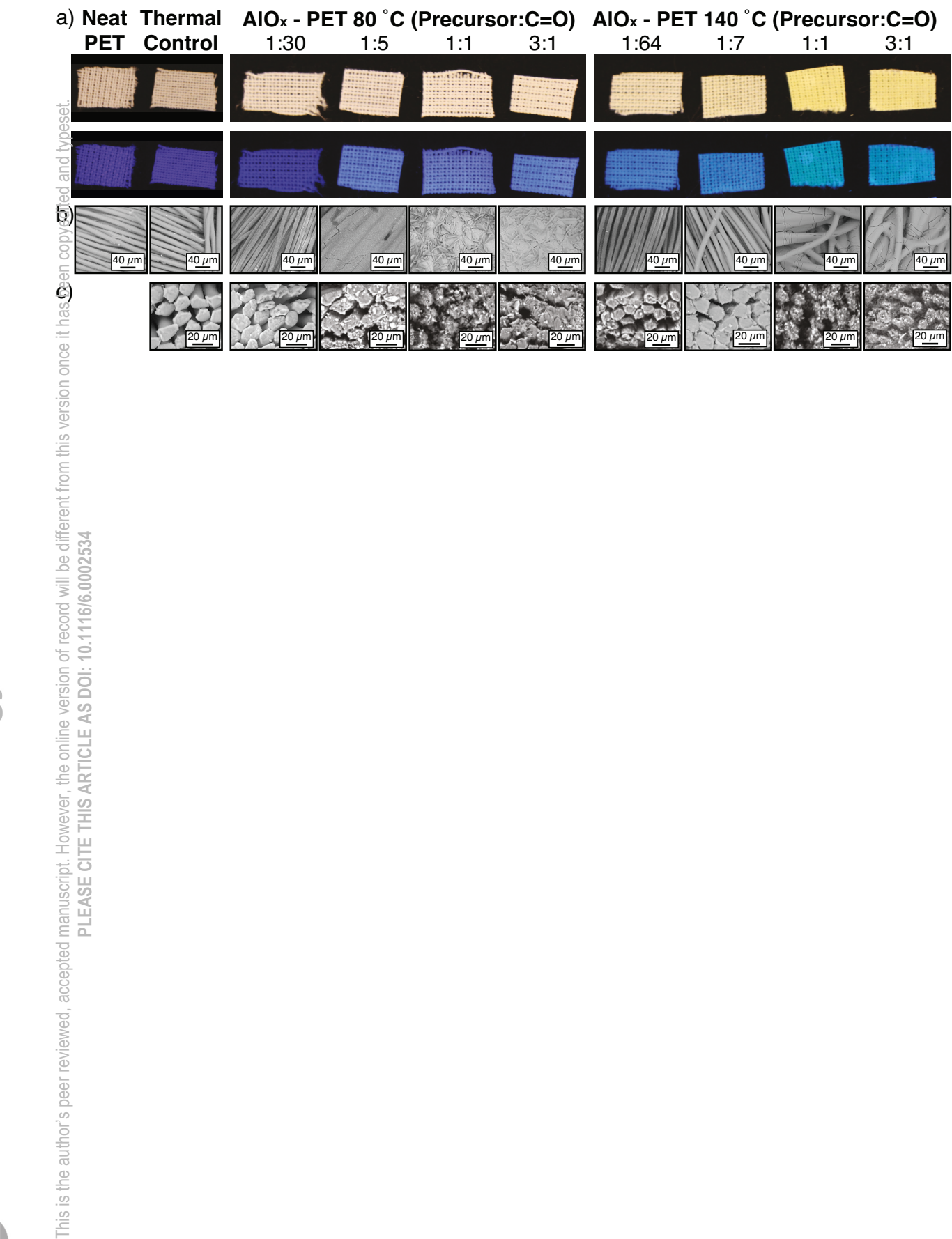
## Journal of Vacuum

This is the author's peer reviewed, accepted manuscript. However, the online version of record will be different from this version once it has been copyedited and typeset. Science & Technology A

PLEASE CITE THIS ARTICLE AS DOI: 10.1116/6.0002534

 $a)^{1.0}$ TMA Exposure Step 80 °C \*... ( )**%**#%\$\$#. i 0.8 3:1 Precursor:C=C 0.6 1:1 Precursor:C=O 0.4 VPI Chamber 0.2 PET fabric 0.0 2 3 ( + #&- "\$\* **b)**30 80 °C . 25 140 °C 20 15 10 5 \*lines are drawn to guide the eye 0 Precursor:C=O 3 1

### Journal of Vacuum Science & Technology A





# ACCEPTED MANUSCRIPT

## Journal of Vacuum

Science & Technology A

This is the author's peer reviewed, accepted manuscript. However, the online version of record will be different from this version once it has been copyedited and typeset.

PLEASE CITE THIS ARTICLE AS DOI: 10.1116/6.0002534



